J Mater Sci (2022) 57:21828–21840

Metals & corrosion

Surface tension of liquid Ti, V and their binary alloys measured by electromagnetic levitation

B. Reiplinger[1,*], Y. Plevachuk[2], and J. Brillo[1]

[1] Institut Für Materialphysik im Weltraum, Deutsches Zentrum Für Luft- Und Raumfahrt (DLR), 51170 Cologne, Germany
[2] Department of Metal Physics, Ivan Franko National University of Lviv, Lviv 79005, Ukraine

Received: 30 August 2022
Accepted: 18 November 2022
Published online: 6 December 2022

ABSTRACT

The surface tension of the liquid Ti-V system is systematically measured using the oscillating drop technique during electromagnetic levitation. Temperature- and compositional dependence are both investigated. The entire compositional range is covered. A linear decrease with increasing temperature is found for the pure elements as well as for all investigated alloys. The surface tension generally increases with increasing V-content. The obtained data are in good agreement with the Butler model for the ideal solution. Additionally, the Butler model for the regular solution was evaluated in the context of the obtained surface tension data. In contrast to many other Ti-based alloys, the Butler model for the regular solution yields no additional benefit for Ti-V, since there is only a neglectable small deviation between the calculations for the ideal and regular solution. Segregation effects are modeled using the Butler equation for an ideal solution. The findings are discussed considering already existing trends for the mixing behavior of liquid Ti-alloys. The results strongly suggest, that the Ti-V system obeys in general the ideal solution law.

Introduction

Motivation

Titanium-based alloys are subject to steadily increasing interest in both, a wide variety of applications, ranging from aerospace [1, 2] over additive manufacturing [3, 4] to biomedical implementations [5, 6] and as a subject of fundamental research [7, 8]. Commercially most relevant are α–β titanium alloys, i.e., alloys with minor additions that stabilize the low-temperature close-packed hexagonal α-phase of titanium as well as those which stabilize the bcc β-phase [9]. Aluminum is the most prominent α-stabilizing element, while vanadium is one of the most frequently used β-stabilizing elements [9]. Therefore, the Al-Ti-V system is of great significance, including many industrially used titanium alloys. $Al_6Ti_{90}V_4$, often referred to as Ti64, is the most established example of these alloys, finding wide spread

Handling Editor: P. Nash.

Address correspondence to E-mail: Benedikt.Reiplinger@dlr.de

https://doi.org/10.1007/s10853-022-07995-y

utilization as medical implant material [10], additive manufacturing feedstock [11], aerospace construction material [12] and many more.

With increasing industrial use, the interest in thermophysical properties of the Al-Ti-V system also rises. Therefore, recently different studies investigated the thermophysical properties of several selected Ti-based alloys of high industrial interest, such as the Ti64 [13] alloy or γ-TiAl-based alloys [14]. The liquid phase is hereby crucial. Precise knowledge of thermophysical properties of the liquid phase—such as density, viscosity and surface tension—are required for modeling and design of metallurgical processes [15] like casting or additive manufacturing processes [16] such as selective laser melting (SLM) and electron beam melting (EBM). Additionally, thermophysical properties are often the foundation of understanding the basic interaction mechanisms in multicomponent alloy systems. Thus, it is very surprising that, despite of the importance of the Al-Ti-V systems, only very few systematic data exist on the pure binary and ternary subsystems, except the results already produced in previous studies at DLR [17–22].

These previous investigations at our group focused on the Al-Ti system, its thermophysical properties, and its interactions with oxygen [17–20]. Recently, we expanded these works toward the liquid Ti-V system [21] in order to characterize and understand the complete Al-Ti-V ternary system by progressing its investigation by means of its binary margins.

Liquid Ti-V shows the behavior of an ideal solution regarding density and molar volume [21]. It is therefore interesting to examine if such an ideal behavior is also observed for other thermophysical properties, such as the surface tension.

Thus, the purpose of the present work is twofold. On the one hand, we aim to provide systematic and reliable surface tension data for the complete Ti-V liquid system in order to complete existing datasets for this system [21]. The second aim of the present work is to gather further insights into the general mixing behavior of this interesting and important class of alloys.

The high melting temperatures of titanium (1941 K) and vanadium (2183 K) [23] as well as their high chemical reactivity possess severe challenges for conventional container-based surface tension measurement techniques at elevated temperatures. Thus, electromagnetic levitation (EML) as a container-less method is applied in the present work in order to handle these challenges and to allow for a precise surface tension measurement over a broad temperature range without the risk of contamination from any container walls [24]. The measured data will be evaluated using the Butler equation [25] as thermodynamic model.

Butler equation

In the Butler model [25], surface and bulk are considered as two distinct thermodynamic phases, each having their own composition and chemical potential. The chemical potential of the surface phase has an additional term which depends on the surface tension γ. If the two phases are in equilibrium with each other, their chemical potentials are equal, resulting in the Butler equation. For an ideal solution, the latter can be written in following form [26, 27]

$$\gamma = \gamma_i \frac{\omega_i^0}{\omega_i} + \frac{RT}{\omega_i} ln\left(\frac{x_i^S}{x_i^B}\right) \tag{1}$$

In this equation, γ_i represents the surface tension of pure element i and x_i^S and x_i^B represent its mole fraction in the surface- and the bulk phase, respectively. R is the molar gas constant, R = 8.314 J/mol/k and ω_i^0 is the molar surface area of the pure, unmixed component i and ω_i is the corresponding partial molar surface area of component i in the mixture. The latter has been identified by Kaptay as an immanent property [26]. It is defined as.

$$\omega_i \equiv \frac{A_i}{n_i}, \tag{2}$$

if n_i denotes the number of moles of species i in the surface area and A_i is the size of the surface covered by it under the condition that the total surface area is $A = \sum_i A_i$. ω_i and ω_i^0 are related to the molar volume V_{mol} of the solution [26]. In the case of a binary alloy (i,j) this relation reads [27]:

$$\omega_i = \omega_i^0 + \left(x_j^S\right)^2 L_\omega \tag{3}$$

with

$$\omega_i^0 = f \cdot N_{Av}^{\frac{1}{3}} \left(V_i^0\right)^{2/3}$$

$$L_\omega = f \cdot N_{Av}^{\frac{1}{3}} (L_V)^{2/3} \tag{4}$$

whereas f = 1.0 is a geometrical factor, whose value is

chosen in agreement with Ref. [28]. N_{av} is the Avogadro number and V_i^0 is the molar volume of pure substance i. L_ω is an interaction constant that is related via Eq. (4) to the interaction constant of the molar volume L_v that determines the excess volume $V^E = x_i x_j L_V$. If the excess volume is zero or can be neglected, as is the case with liquid Ti-V [21], Eq. (3) turns into the following:

$$\omega_i = \omega_i^0 = f \cdot N_{Av}^{\frac{1}{3}} \left(V_i^0\right)^{2/3} \tag{5}$$

Thus, for Ti-V, the Butler equation of the ideal solution can be simplified so that it attains the usual form:

$$\gamma = \gamma_{Ti} + \frac{RT}{\omega_{Ti}^0} ln\left(\frac{x_{Ti}^S}{x_{Ti}^B}\right) = \gamma_V + \frac{RT}{\omega_V^0} ln\left(\frac{1 - x_{Ti}^S}{1 - x_{Ti}^B}\right) \tag{6}$$

Under the condition that γ_{Ti}, γ_V, $V^0{}_{Ti}$ and $V^0{}_V$ are known, Eq. (6) can be solved numerically for given $x^B{}_{Ti}$ and T using some standard algorithm. As result, γ and $x^S{}_{Ti}$ are obtained for a given temperature and bulk composition. When the calculation is carried out at various different temperatures, also the temperature coefficient γ_T can be obtained.

For a non-ideal system, where ${}^E G \neq 0$, Eq. (6) expands to

$$\gamma = \gamma_{Ti} + \frac{RT}{\omega_{Ti}^0} ln\left(\frac{x_{Ti}^S}{x_{Ti}^B}\right) + \frac{1}{\omega_{Ti}^0}\left({}^E G_{Ti}^S(T, x_{Ti}^S, x_V^S) - {}^E G_{Ti}^B(T, x_{Ti}^B, x_V^B)\right) \tag{7}$$

with ${}^E G_{Ti}^S$ and ${}^E G_{Ti}^B$ being the excess free energies of titanium in the Ti-V system, for the surface and the bulk phase. While the excess free energies for the bulk phase can be determined using thermodynamic assessments, they are not so easily obtained for the surface. For our work we used a procedure described in more detail in [29], calculating the excess free energy of the surface from those of the bulk, as follows:

$${}^E G_{Ti}^S(T, x_{Ti}^S, x_V^S) \approx \xi {}^E G_{Ti}^B(T, x_{Ti}^S, x_V^S) \tag{8}$$

Here ξ is a geometrical factor to incorporate the coordination of the surface phase atoms. Finally, the excess free energy was calculated following a Redlich–Kister polynomial of the form

$${}^E G_{Ti}^B(T, x_{Ti}^S, x_V^S) = x_{Ti}^B x_V^B \sum_v {}^v L_{Ti,V}(T) * \left(x_{Ti}^B - x_V^B\right)^v \tag{9}$$

The parameters used are taken from Ref. [30] and listed in Table 1. A more detailed description for the Butler model of the regular solution can be found in [29, 31, 32].

Experimental method

Electromagnetic levitation

Electromagnetic levitation (EML) is based on the principle that an alternating inhomogeneous magnetic field induces eddy currents inside the electrically conducting sample which, apart from an inductive heating and melting of the specimen, also leads to its stable positioning against gravity due to the action of Lorenz-forces. The method is described in detail in reference [24].

Experiments are performed in an inert He, Ar (99.9999 vol pct. purity) mixture atmosphere of 750 hPa and inside a vacuum chamber. The chamber has been evacuated prior to the actual experiment down to a pressure of at least 10^{-6} hPa in order to remove residual gas components such as H_2O, O_2, CO, CO_2 and hydrocarbons. Thus, the contamination risk of the sample is further reduced. In the beginning of an experiment, the sample is located on a ceramic sample holder and introduced into the water-cooled levitation coil to which then an alternating current in the order of 200 A is applied with a frequency of approximately 250 kHz. As soon as the sample levitates, the sample holder is withdrawn.

The samples are nearly of spherical shapes with typical diameters of 7 mm. Depending on the material's density, the masses of the sample vary between 0.9 to 1.3 g.

In electromagnetic levitation, heating and positioning are not decoupled. Thus, to adjust the temperature by counter-cooling of the sample, a variable flow of He- or Ar- gas is admitted to it through an alumina nozzle. In addition, the temperature can be adjusted within certain limits by cautiously reducing the generator power.

Table 1 Redlich–Kister parameters for liquid Ti-V taken from Ref. [30]

Parameter	Value [Jmol^{-1}]
${}^0L_{Ti,V}$	1400
${}^0L_{Ti,V}$	4100

The droplet temperature is determined by use of a single-color pyrometer. Since the emissivity of the specimen is generally unknown, a correction of the pyrometer signal is necessary to obtain the actual temperature T of the sample. Assuming that the effective emissivity at constant wavelength does not significantly vary over the temperature range of the measurement, T can be approximated using the equation below, which is derived from Wiens' law [33]:

$$\frac{1}{T} = \frac{1}{T_P} - \frac{1}{T_{P,L}} + \frac{1}{T_L} \tag{7}$$

Here, T_P is the uncorrected pyrometer signal, T_L is the true liquidus temperature and $T_{L,P}$ denotes the liquidus temperature observed in the pyrometer signal.$T_{L,P}$ manifests itself in the pyrometer signal as a kink at the end of the melting plateau where the melting process is concluded. T_L is usually taken from an independent measurement. In this work, it is read from the phase diagram reported in Reference [23]. The liquidus temperature for each composition, as well as the measurement temperature range from the minimum temperature T_{min} to the maximum temperature T_{max} are listed in Table 2.

Oscillating drop method

The oscillating drop method has been applied in many previous works to accurately measure the surface tension of a molten droplet in levitation [17, 24, 31, 32, 34–37]. For this technique, a high-speed camera records a series of 6000 frames at a frequency of 400 fps of the sample from a top view position. Afterward the frames are analyzed by a custom software extracting the frequency spectra of two perpendicular radii $r_x(\omega)$ and $r_y(\omega)$, as well as three translational frequencies $\omega_{x,}\omega_y$ and ω_z of the sample center of mass.

Table 2 Liquidus temperature T_L, minimum temperature T_{min} and maximum measurement temperature T_{max} for each investigated composition

Composition	T_L [K]	T_{min} [K]	T_{max} [K]
Ti	1941	1825	2218
$Ti_{87.5}V_{12.5}$	1913	1911	2274
$Ti_{75}V_{25}$	1893	1825	2236
$Ti_{69}V_{31}$	1881	1857	2235
$Ti_{50}V_{50}$	1913	1752	2170
$Ti_{37.5}V_{62.5}$	1937	1860	2193
$Ti_{25}V_{75}$	2023	1873	2333
$Ti_{12.5}V_{87.5}$	2113	1964	2320
Ti_5V_{95}	2173	1905	2258
V	2183	1957	2289

The liquidus temperatures inferred from the phase diagram introduced in [23]

In a force-free environment the surface tension γ of a spherical, non-rotating droplet can be correlated to the Rayleigh frequency ω_R via the following equation [24], if M is the mass of the droplet:

$$\omega_R^2 = \frac{32\pi}{3M}\gamma \tag{8}$$

It can be shown, that the Rayleigh frequency corresponds to an $l = 2$ mode with fivefold degeneracy $|m| \leq l$ under the condition of the spherical symmetry. However, on earth, the droplets are no longer force-free and in the electromagnetic levitation environment, the spherical symmetry needs to be replaced by a cylindrical symmetry. Therefore, the degeneracy is lifted and the Rayleigh frequency splits into a set of three distinct frequencies $\omega_{2,\pm2}$, $\omega_{2,\pm1}$, and $\omega_{2,0}$ where the $m = \pm 2$- and the $m = \pm 1$-modes are still twofold degenerate [38]. This degeneracy, however, is also removed, if the droplet rotates slightly, which is usually the case. It is important to note, that the frequency of these sample rotations needs to be very small compared to the Rayleigh-frequency (≤ 5 Hz) since sample rotations of frequencies in the order of the Rayleigh-frequency can greatly impair the measurement as will be explained in more detail later. As a result, five distinct frequencies, ω_m are observed in the spectrum. The surface tension, γ, is calculated from these frequencies using the formula of Cummings and Blackburn [32] or one of its variants:

$$\gamma = \frac{3M}{160\pi}\left(\sum_{m=-2}^{2}\omega_m^2 - 9.5\Omega^2 - 1.5\left(\frac{g}{a}\right)^2\Omega^{-2}\right) \tag{9}$$

Here, M is the mass of the sample, a is its radius, and g is the gravitational acceleration. In Eq. (9), the parameter Ω corrects for the magnetic pressure. It is calculated from the three translational frequencies, $\omega_{X,Y,Z}$, corresponding to the horizontal and vertical movements of the sample: $\Omega^2 = 1/3(\omega^2{}_X + \omega^2{}_Y + \omega^2{}_Z)$. Depending on the mass of the sample, the frequencies of the translational movements are

typically between 5 and 20 Hz, whereas as a rule of thumb, $\omega_Z \approx 2\omega_X \approx 2\omega_Y$. The frequencies ω_X and ω_Y are determined from the horizontal motion of the droplet center, while ω_Z is extracted from the spectrum of the apparent droplet area, which changes with vertical movement of the sample due to the changing distance between the sample and the high-speed camera.

Sample material and preparation

In order to sufficiently map the Ti-V system, 10 different alloy compositions equally covering the whole compositional range, including the pure elements, were prepared. As raw materials, titanium from AlphaAesar with a purity of 99.999% as well as vanadium from Hauner GmbH with a purity of 99.99% were used. After cutting the desired weight for each element, the raw materials were alloyed together in an arc-furnace under a protective argon atmosphere. Before and after alloying the samples were cleaned in an isopropanol ultrasonic bath to remove any residual surface impurities. The resulting samples had a near spherical shape with a diameter of approximately 7 mm.

Different sources of quantified experimental errors and their potential impact on the surface tension measurement are given in Table 3. Mass loss due to sample evaporation during levitation was kept below 0.5% by measuring the mass of each sample before and after levitation and discarding all samples that showed a mass loss of $\geq 0.3\%$. Sample contamination was minimized by the use of high purity raw materials and an inert protective atmosphere (He, Ar) during alloying and levitation. Special attention is hereby paid to the oxygen influence on the measurement, since already a small oxygen content can have a major impact on the surface measurement of a liquid metal. Previous research in our group [1] has shown, that the implementation of the mentioned purity conditions, such as the high purity raw material and the protective argon atmosphere during all sample preparation as well as measurement steps, keeps the oxygen content during the measurement neglectable small. In order to obtain an estimate on how much oxygen is introduced into the sample during the levitation, an oxygen analysis on pure vanadium was done before and after the levitation experiment. The measurements were carried out by the analytical services of the 'Elektrowerk Weisweiler GmbH'. Two identical samples of pure vanadium were prepared. Afterward one of these samples was processed in the electromagnetic levitation furnace while the second sample was not. The oxygen content of both samples was subsequently analyzed. The 'as prepared' sample showed 0.08 at. − % oxygen, while the 'processed' sample showed 0.1 at. − %. A similar approach was taken for pure titanium in [20] and [39], where the oxygen content of pure titanium samples was analyzed for different processing durations. There, an increase from 0.079 at. − % for the 'as prepared' sample, to 0.23 at. − % for the sample processed for 90 min. was observed. In both cases a slight increase in oxygen content can be noted. Even for pure titanium the oxygen content after processing in the electromagnetic levitation furnace still lays well below the threshold of around 1 at. − % at which oxygen has a noticeable impact on the surface tension as shown by [20] and [39]. However, the influence of oxygen on thermophysical properties and surface tension in particular is far too complex to just be neglected. Therefore, consecutive investigations are currently carried out at our group, examining the influence of different oxygen contents on

Table 3 Error sources as well as their impact on the surface tension measurement for the oscillating drop method

Error source	Parameter	Order of magnitude	Impact on surface tension
Evaporation	m	$\leq 0.3\%$	severe
Sample rotation	ω_m	$\leq 2.5\%$	severe
Temperature reading	T	$\leq 1\%$	uncritical
Lateral sample movements	Ω	$\leq 1.25\%$	uncritical
Purity conditions	x_O	$\leq 1\%$	severe
Edge detection	r_x, r_y	$\leq 0.5\%$	uncritical

T denotes the temperature, m the sample mass, ω_m the modes of the Rayleigh frequency, x_O the mole fraction of oxygen, Ω a correction parameter for the magnetic pressure and r_x and r_y the two perpendicular radii of the recorded sample.

various Ti and V alloys and their thermophysical properties. First results indicate a similar behavior for pure liquid V and Ti. All this leads to the assumption, that even though there is a slight increase in oxygen content over the course of the measurement, it is not big enough to have a major impact on the surface tension.

Additionally, sample rotations with a frequency in the same order of magnitude as the Rayleigh frequency can greatly impair the surface tension measurement, as they superimpose the frequency spectrum, usually with a much higher intensity than the surface oscillations. Strong rotations of the sample during levitation, make an identification of five distinct peaks corresponding to the Rayleigh Frequency impossible. Instead, only one major peak at the rotation frequency can be observed. The coil design must therefore be carefully adjusted in order to suppress any sample rotations during the levitation process. An estimation of the measurement error can be done by investigating the propagation of uncertainty of all parameters in Eqs. (8) and (9). The deviation in temperature was assumed to be ± 10 K, the maximum mass loss $\geq 0.3\%$ and the error for the frequency reading ± 0.5 Hz. These assumptions lead to an estimated error in surface tension of $\leq 5\%$. An experimental validation for these assumptions can be found in [29].

Results and discussion

Pure elements

Surface tension data γ of pure liquid Ti and V are plotted versus temperature T in Figs. 1 and 2, respectively.

For liquid Ti (Fig. 1) data are measured over a temperature range from 1800 to 2300 K. This includes a maximum undercooling of 140 K below the liquidus temperature T_L = 1941 K. Over this interval, the measured surface tensions range from 1.47 N/m at a temperature of 2305 K to 1.53 N/m at 1823 K. Within the error bars of ± 5%, the results are in good agreement with the displayed results from literature [17, 40], although they are by a little more than half a percent lower.

The surface tension follows a linear law with a negative slope. This is represented by the following equation, whereas γ_L denotes the surface tension at the liquidus temperature T_L and γ_T denotes the temperature coefficient, i.e., the slope:

$$\gamma(T) = \gamma_L + \gamma_T(T - T_L) \quad (10)$$

Fitting Eq. (10) to the data in Fig. 1 yields γ_L = 1.52(± 0.01) N/m and γ_T = − 1.8(± 0.3)·10^{-4} N·m^{-1} K^{-1}, see Table 4.

In the case of liquid V, Fig. 2, the temperature range extends from 1950 to 2300 K. Thus, a deep undercooling of the liquidus temperature, T_L = 2183 K, by more than 200 K is evident. The measured surface tensions range from 1.92 N/m at

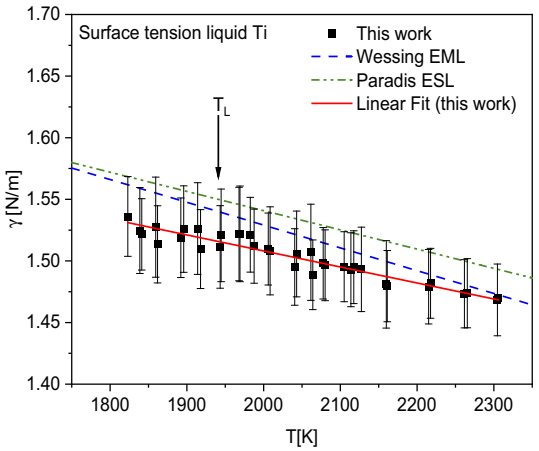

Figure 1 Surface tension of liquid titanium versus temperature (symbols). The solid line represents the fit from Eq. (10). The dashed line represents data measured by Wessing [17] and the dash-dotted line represents data measured by Paradis [41] for comparison.

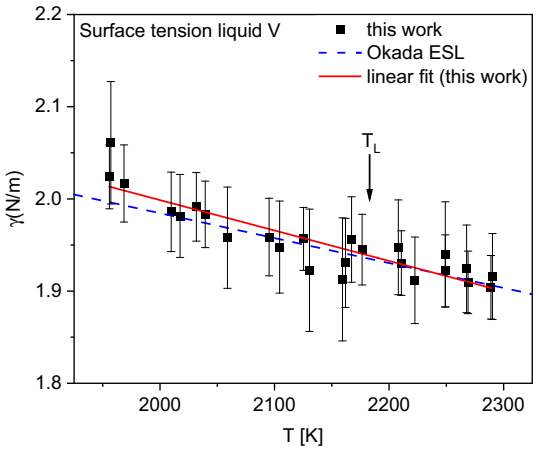

Figure 2 Surface tension of liquid vanadium versus temperature (symbols). The solid line represents the fit from Eq. (10). The dashed line represents data measured by Okada [42] et al. for reference.

Table 4 Parameters T_L, γ_L, γ_T for pure elements titanium and vanadium with the corresponding uncertainties

Element	T_L [K]	γ_L [N/m]	γ_T [N/m]	γ (2100K) [N/m/K]	Reference	Method
Ti	1941	1.52 ± 0.01	− 1.77 ± 0.3	1.4611	This work	EML
		1.56 ± 0.02	− 1.65 ± 0.95	1.500	[17]	EML
		1.557 ± 0.08	− 1.56 ± 0.8	1.503	[41]	ESL
V	2183	1.94 ± 0.07	− 3.29 ± 0.7	1.967	This work	EML
		1.935 ± 0.09	− 2.7 ± 0.9	1.903	[42]	ESL
		1.950	–	–	[48]	Pendant drop

Additionally, the isothermal surface tensions for 2100 K are shown. Reference data for different measurement methods are provided

2290 K to 2.06 N/m at 1957 K. Within the error bars of ± 5% the results are in excellent agreement with those of Okada [42]. Again, γ linearly decays with temperature. Fitting of Eq. (10) yields γ_L = 1.94(± 0.07) N/m and γ_T = − 3.3(± 0.07)·10^{-4} N·m^{-1} K^{-1}, see Table 4.

Alloys

In the case of the binary Ti-V alloys, the temperature dependent surface tension data γ (T) are shown in Fig. 3. For the sake of completeness, the figure also shows the data of the pure elements. An overall temperature range from ≈1800 K to ≈2300 K is covered for all samples. Similar to the cases of the pure elements, γ is obtained as linear functions of T with negative slopes. The corresponding parameters γ_L and γ_T, obtained from fitting Eq. (10), are listed in Table 5. As a general trend, the surface tension

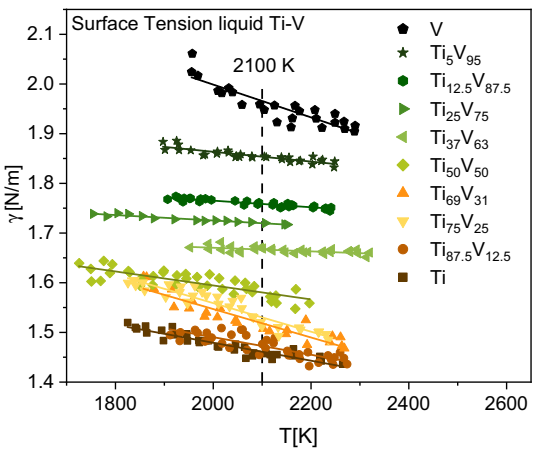

Figure 3 Surface tension of liquid Ti, V and Ti-V binary alloys versus temperature. The solid lines represent the fits according to Eq. (10). The dashed line marks 2100 K, a reference point for the compositional dependence.

decreases with increasing Ti bulk mole fraction x^B_{Ti}. In order to further discuss this dependence on concentration, the surface tension at T = 2100 K is calculated using Eq. (10) and the parameters in Table 5. This temperature is marked in Fig. 3 by a vertical line. It was chosen because, for all alloys, it lies in the center of the investigated temperature intervals.

The result γ (2100 K) is plotted in Fig. 4 versus x^B_{Ti}. Obviously, there is a monotonous decrease of γ with x^B_{Ti} following a moderately convex curve from 1.97 N/m corresponding to pure liquid V down to 1.46 N/m for pure liquid Ti. The non-linear shape of the curve indicates already, that the surface is slightly enriched in Ti, since pure Ti has the lower surface tension of the two components.

In Fig. 3, the steepness of the curves, i.e., the temperature coefficient γ_T, also varies with composition in a way, that the γ-T curves in Fig. 3 are steeper for the pure elements and flatter for the alloys. This is shown in detail in Fig. 5 where γ_T is plotted versus x^B_{Ti}. Starting on the side of pure vanadium in the figure, γ_T steeply increases with x^B_{Ti} from initially − 3.3·10^{-4} N·m^{-1} K^{-1} to − 9.8·10^{-5} N/m/K at x^B_{Tii} = 5 at. − %, i.e., within the first few at. − % of Ti. The further increase is much slower and there appears to be a maximum of γ_T at x^B_{Ti} = 37 at. − % where γ_T = − 3.64·10^{-5} N·m^{-1} K^{-1}. Upon further increase of x^B_{Ti} the temperature coefficient γ_T is decreasing slowly but monotonously with respect to the margin of scatter until the value of pure Ti, − 1.80·10^{-4} N·m^{-1} K^{-1}, is reached. This behavior indicates a smaller surface entropy of the alloys as compared to the pure elements which, interestingly, may be interpreted as that there is a higher degree of order.

The results in Figs. 4 and 5 can be compared to the Butler equation, Eq. (6). For this purpose, the

Table 5 Parameters T_L, γ_L, and γ_T for every composition examined in the Ti-V system

x^B_{Ti} [at. − %]	T_L [K]	γ_L [N/m]	γ_T [10^{-4} N·m^{-1} K^{-1}]	Γ(2100 K)[N/m]
0	2183	1.94 ± 0.07	− 3.29 ± 0.7	1.967
5	2173	1.85 ± 0.02	− 9.78 ± 0.25	1.855
12.5	2113	1.76 ± 0.01	− 6.64 ± 0.5	1.759
25	2023	1.72 ± 0.01	− 5.49 ± 0.4	1.7197
37.5	1937	1.67 ± 0.02	− 3.64 ± 0.43	1.6667
50	1913	1.61 ± 0.08	− 1.41 ± 0.42	1.5804
69	1881	1.56 ± 0.05	− 1.57 ± 0.39	1.5248
75	1893	1.53 ± 0.04	− 1.12 ± 0.35	1.50633
87.5	1913	1.51 ± 0.04	− 1.77 ± 0.5	1.47268
100	1941	1.52 ± 0.01	− 1.77 ± 0.3	1.4611

Additionally, the isothermal surface tension for 2100 K is shown

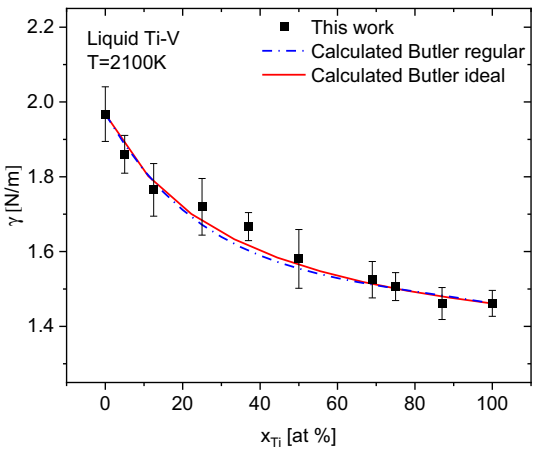

Figure 4 Isothermal surface tension of liquid Ti-V at 2100 K as a function of the titanium bulk mole fraction x^B_{Ti}. The red line represents the surface tension of an ideal solution calculated from Eq. (6). For comparison, the blue dashed line shows the surface tension calculated for a regular solution, using the Butler model analogous to Ref. [43].

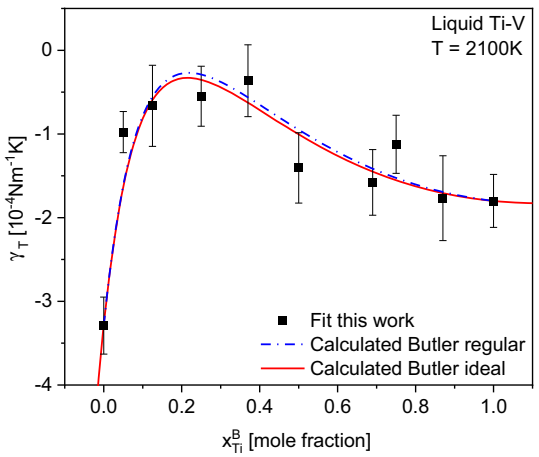

Figure 5 Temperature coefficient γ_T versus the titanium bulk mole fraction x^B_{Ti}. The solid line represents the calculation utilizing the Butler model, Eq. (6), for the ideal solution. The dashed line represents the regular solution.

temperature dependent data of V^0_{Ti} and V^0_V, needed in Eq. (5), are derived from the corresponding density data in our previous work on Ti-V [21]. They are listed in Table 6 together with corresponding volume expansion coefficients β. The latter are used in order to calculate the Butler equation at different temperatures. In addition, γ is calculated for T = 2090 K and for T = 2110 K, so that the temperature coefficient γ_T is obtained as $\gamma_T = (\gamma(2110\ K) - \gamma(2090\ K))/20$ K.

Thus, Figs. 4 and 5 also show the calculations, Eq. (6), of γ at 2100 K and γ_T as functions of the Ti bulk mole fraction x^B_{Ti}. Obviously, the agreement with the experimental data is excellent. In Fig. 4, the Butler equation exactly reproduces the data and it needs to be emphasized at this point, that Eq. (6) is purely predictive and that no kind of fitting or adjustment to the data is involved. For comparison, the surface tension calculated for the regular solution using the Butler equation is also included. The calculations for the regular solutions have been done analogous to Ref. [43]. Using the Redlich–Kister coefficients from [30], the calculated excess Gibbs energies are very small and thus the difference between the calculations for the ideal and regular solution are neglectable. This strengthens the findings of Ti-V showing near ideal behavior in regard to the surface tension. However, since the excess Gibbs energies are different from zero, the mixing behavior in the liquid phase is not exactly ideal in a strict sense, but they are extremely close to ideal, so that there is no difference from a practical point of view.

Table 6 Parameters for pure Ti and V used in order to calculate the Butler equation,

i	T_L [K]	ρ_L [g·cm^{-3}]	ρ_T [10^{-4} g·cm^{-3} K^{-1}]	ρ(2100 K) [g·cm^{-3}]	$V_i^0(2100K)$ [cm^{3}mol^{-1}]	β [10^4cm^{3}mol^{-1} K^{-1}]
Ti	1941	4.21	− 3.46	4.155	11.52	0.833
V	2183	5.55	− 6.01	5.454	9.340	1.102

Equation (6). The parameters are taken or derived from our previous work [21]

In Fig. 5, the values of γ_T are also nicely reproduced qualitatively, as well as quantitatively. The calculated curve highlights details in the experimental data, which would not have so easily become obvious without the calculation: For instance, it shows that the true position of the maximum is at x^B_{Ti} = 20 at. − % rather than at 37 at. − % as indicated by the data and also, there seems to be an inflection point at around x^B_{Ti} = 40 at. − % where the curvature of the graph changes from concave to convex.

In addition to the surface tension, the Butler equation can also predict the surface Ti mole fraction x^S_{Ti}. This is shown in Figs. 6 and 7 for a constant temperature T = 2100 K. Figure 6 compares the segregation of three different titanium alloys, namely Al-Ti, Cu-Ti and Ti-V. For this comparison, the model that reproduces the measured surface tension data best was used to calculate the surface composition of the respective alloy. Subsequently the surface

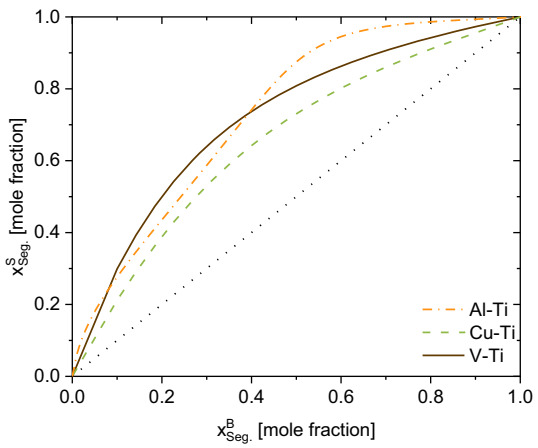

Figure 6 Calculated mole fraction $x^S_{Seg.}$ of the segregating species in the surface layer for different Ti-based alloys at 2100 K as a function of the bulk mole fraction $x^B_{Seg.}$. For each composition the Butler model was chosen, that represents the respective measured data best. For Al-Ti and Cu-Ti this is the case for the Butler model of the regular solution. For Ti-V this is the case for the ideal solution Butler model.

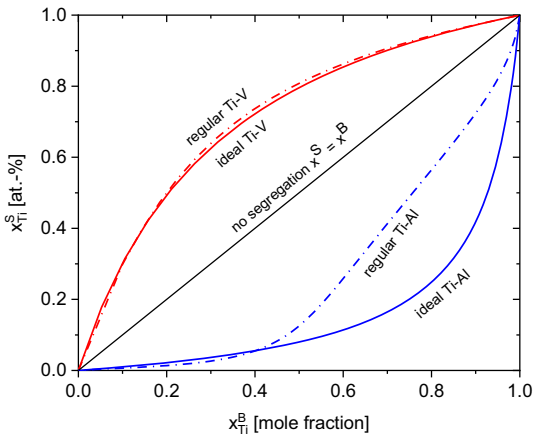

Figure 7 Calculated mole fraction $x^S_{Ti.}$ of titanium in the surface layer for Ti-V compared to Al-Ti at 2100 K as a function of the bulk mole fraction $x^B_{Ti.}$. For each alloy the Butler model for the ideal as well as the regular solution is displayed. The solid line represents the ideal solution, while the dashed line represents the regular solution.

concentration of the segregating species was plotted against the bulk concentration of the segregating species. The diagram displays a convex curve for Ti-V with a moderately strong increase on the left hand side in the figure so that x^S_{Seg} ≈ 80 at. − % is already reached at x^B_{Seg} ≈ 50 at.-%. In the case of Ti-V, the segregating species is Ti ($x^s_{Seg.} = x^s_{Ti.}$), thus, in liquid Ti-V, the surface is enriched in Ti. This so called (surface-)segregation obviously takes place already if, as in the case of present study, the ideal solution model is considered. The phenomenon can be interpreted in terms of overall energy minimization. Thus, by segregation of the component with the smaller surface free energy, Ti in the case of Ti-V, the total energy of the system is minimized. Consequently, the effect is larger in systems with a positive excess free energy $^EG > 0$, i.e., where there is a tendency to demix [29]. In contrast to this, attractively mixing systems where $^EG < 0$ exhibit only weak segregation [29].

In Fig. 7, the surface concentration of titanium is shown as a function of the bulk titanium concentration for both Ti-V and Al-Ti. Calculations using the Butler model for both, the ideal and the regular solution are shown for either system. Ti-V shows moderate segregation compared to the strong segregation of Al-Ti. Additionally, for the Ti-V system the surface is enriched in Ti, while the opposite is true for Al-Ti. However, in the case of Al-Ti, the experimentally measured data are not adequately reproduced by the Butler equation for the ideal solution. Instead the Butler model for the regular solution needs to be implemented, which shows a significantly weaker segregation effect, especially at mole fractions ≥ 0.5. For Ti-V the deviation between both models is neglectable small.

Discussion

The fact, that the surface tension of the Ti-V system can be well be reproduced by the Butler-equation for the ideal solution, see Figs. 4 and 5, is remarkable, because it agrees with our earlier observation that also the molar volume of liquid Ti-V obeys the ideal solution model [21]. In our investigations regarding the density and molar volume of the Ti-V system we suggested the similarities in electronic structure of Ti and V, both being d-transition metals, as a possible indicator for the lack of excess volume in the system. The same argument can be applied when considering the surface tension of liquid Ti-V. The proximity of Ti and V in the periodic table may imply, that the electronic structure does not change dramatically upon mixing, indicating an overall ideal behavior. The present work confirms this hypothesis for the surface tension, since no significant excess surface tension was evident.

Brillo [29] ordered several binary and ternary metallic systems in two groups regarding their behavior upon mixing, as well as their excess surface tension. Systems of the first group tend to demix, showing a positive excess free energy ${}^{E}G > 0$, a negative excess surface tension and a strong segregation behavior while systems belonging to the second group tend to mix, showing negative excess free energy ${}^{E}G < 0$, a positive excess surface tension. All titanium alloys investigated at our institute, much like most titanium alloys, show a negative excess free energy and therefore fit in the second group. Even though for Ti-V the excess free energy calculated from [43] almost zero, it is still negative. It can be seen, that Ti-V shows moderate segregation, similar to that of the other titanium alloys displayed.

In an effort to illustrate the ideality of the Ti-V system, the segregation of the Ti-V system was compared to that of the Al-Ti system in Fig. 7. Here two things become evident. Firstly, for Ti-V titanium is the segregating species, while for Al-Ti aluminum segregates to the surface. Secondly, there is a significant difference between the calculations of the Butler model for the ideal and the regular solution in case of Al-Ti while the difference is neglectable small for the Ti-V system. So, while the general magnitude of the segregation seems to be related to the excess free energy as classified in [29], the segregating species as well as the ideality of the surface composition seems to be highly dependent on the alloying element for Ti- alloys.

Another sign for liquid Ti-V being an ideal solution is the phase diagram [23] which is characterized by convex solidus- and liquidus lines close together become are tangent to each other in one point, namely the azeotropic point at high temperatures, as well as a miscibility gap at low temperatures. Phase diagrams of this form are exemplary for systems with an ideal behavior in the liquid phase and demixing solid phase [44]. A similar phase diagram, also with an azeotropic point, is exhibited by the Au-Cu system [45] which, similar to Ti-V is regarded as an ideal solution, just as Ag-Au, where the solidus and liquidus lines are lentil-shaped [46] indicating that mixing entropy dominates over the mixing enthalpy. Knowing that Ag-Au, Au-Cu and Ti-V all show almost no excess volume it would be highly interesting to investigate if Ag-Au and Au-Cu also show the same surface tension and segregation behavior as Ti-V.

As shown, existing thermophysical assessments suggest a neglectable small, negative excess free energy ${}^{E}G$ [47] and excess enthalpy ${}^{E}H$ [30] for the Ti-V system. These calculations, combined with the experimental findings of this and our previews work strongly indicate that the liquid Ti-V system overall follows the ideal solution model. Whether other thermophysical properties of the system also follow the ideal solution law should be subject of future studies.

Summary

The oscillating drop technique has been used in electromagnetic levitation in order to systematically investigate the surface tension of the liquid binary Ti-V system over a broad temperature range. A linear decrease of the surface tension with increasing temperature was found for all investigated compositions. Thereupon the isothermal compositional surface tension dependence was developed for the liquid Ti-V system. The experimental data show excellent agreement with the Butler model for an ideal solution. Accordingly, no excess surface tension was evident. The experimental surface tension temperature coefficient is also well represented by the Butler model for the ideal solution. Therefore, the same model was used in order to investigate the segregation behavior of the liquid Ti-V system. It was shown, that the segregation behavior of Ti-alloys strongly depends on the alloying element as well as the excess free energy. Alloys with a positive excess energy show strong segregation, alloys with negative excess energy show rather weak segregation, while the Ti-V system shows moderate segregation effects corresponding to the non-existent excess free energy. The assumption of the Ti-V system as an overall ideal solution was further fortified by the analysis of the surface tension.

Acknowledgements

The authors would like to thank Dr. F. Yang and Prof. Dr. D. Holland-Moritz for their constructive revision of the manuscript.

Funding

Open Access funding enabled and organized by Projekt DEAL.

Declarations

Conflicts of interest There are no known relationships or interests of the authors that influence or bias the submitted work.

References

[1] Boyer R (1996) An overview on the use of titanium in the aerospace industry. Mater Sci Eng 213:103–114

[2] Williams JC, Boyer R (2020) Opportunities and issues in the application of titanium alloys for aerospace components. Metals 10:1–22

[3] Baufeld B, BiestGault OR (2009) Additive manufacturing of Ti–6Al–4V components by shaped metal deposition: microstructure and mechanical properties. Mater Design 31:106–111

[4] Zhang T, Liu C-T (2022) Design of titanium alloys by additive manufacturing: a critical review. Adv Powder Mater 5:1–11

[5] Khorasani AM, Goldberg M, Doeven EH, Littlefair G (2015) Titanium in biomedical applications-properties and fabrication: a review. J Biomater Tissue Eng 5:593–619

[6] Assis SL, Costa I (2007) Electrochemical evaluation of Ti-13Nb-13Zr, Ti-6Al-4V and Ti-6Al-7Nb alloys for biomedicalapplication by long-term immersion tests. Mater Corros 5:329–333

[7] M Mohr, R Wunderlich and H Fecht,(2022) Thermophysical properties of titanium alloys. In metallurgy in space—recent results from ISS. The Minerals, Metals and Materials Series, Springer, Cham

[8] Egry I, Brooks R, Holland-Moritz D, Novakovic R, Matsushita T, Ricci E, Seetharaman S, Wunderlich R, Jarvis D (2007) Thermophysical properties of γ -titanium aluminide: the European IMPRESS project. Int J Thermophys 28:1026–1036

[9] Zhao G-H, Liang X, Xu X, Gamża M, Mao H, Louzguine-Luzgin D, Rivera-Díaz-del-Castillo P (2021) Alloy design by tailoring phase stability in commercial Ti alloys. Mater Sci

Eng A 815:1–10. https://doi.org/10.1016/j.msea.2021.141229
[10] Shah FA, Trobos M, Thomsen P, Palmquist A (2016) Commercially pure titanium (cp-Ti) versus titanium alloy (Ti6Al4V) materials as bone anchored implants—Is one truly better than the other? Mater Sci Eng, C 62:960–966
[11] Liu S, Shin YC (2019) Additive manufacturing of Ti6Al4V alloy: a review. Mater Design 164:107552-1–107623
[12] Uhlmann E, Kersting R, Klein TB, Cruz MF, Borille AV (2015) Additive manufacturing of titanium alloy for aircraft components. Procedia CIRP 35:55–60
[13] Mohr M, Wunderlich RNR, Ricci E, Fecht H (2020) Precise Measurements of thermophysical properties of liquid Ti–6Al–4V (Ti64) alloy on board the international space station. Adv Eng Mater 22:1–10
[14] Nowak R, Lanata T, Sobczak N, Ricci E, Giuranno D, Novakovic R, Holland-Moritz D, Egry I (2010) Surface tension of y-TiAl-based alloys. J Mater Sci 45:1993–2001
[15] Sung S-Y, Kim Y-J (2007) Modeling of titanium aluminides turbo-charger casting. Intermetallics 15:468–474
[16] Wang Q, Zhang W, Li S, Tong M, Hou W, Wang H, Hao Y, Harriso NM, Yang R (2021) Material characterisation and computational thermal modelling of electron beam powder bed fusion additive manufacturing of Ti2448 titanium alloy. Materials 14(23):7359
[17] Wessing JJ, Brillo J (2016) Density, molar volume, and surface tension of liquid Al-Ti. Miner Met Mater Soc ASM Int 48:898–882
[18] Brillo J, Wessing JJ, Kobatake H, Fukuyama H (2021) Molar heat capacity of liquid Ti, Al20Ti80 and Al50Ti50 measured in electromagnetic levitation. High Temp High Press 51(2):145
[19] Brillo J, Wessing JJ, Kobatake H, Fukuyama H (2019) Normal spectral emissivity of liquid Al-Ti binary alloys. High Tempe-High Press 48:423–438
[20] J. J. Wessing, (2018) Thermophysical properties of liquid Al-Ti alloys under the influence of oxygen doctoral dissertation. RWTH Aachen Chair for Foundry Science and Foundry Institute
[21] Reiplinger B, Brillo J (2022) Density and excess volume of the liquid Ti–V system measured in electromagnetic levitation. J Mater Sci 57(16):7954. https://doi.org/10.1007/s10853-022-07090-2
[22] Novakovic R, Giuranno D, Ricci E, Tuissi A, Wunderlichc R, Fecht H, Egry I (2012) Surface, dynamic and structural properties of liquid Al–Ti alloys. Appl Surf Sci 258(7):3269–3275
[23] Murray JL (1981) The Ti−V (Titanium-Vanadium) system. Bull Alloy Phase Diagr 2:48–55
[24] Brillo J, Lohofer G, Schmidt-Hohagen F, Schneider S, Egry I (2006) Thermophysical property measurements of liquid metals by electromagnetic levitation. Int J Mater Prod Technol 26:247–273
[25] Butler JAV (1932) The thermodynamics of the surfaces of solutions. Proc Roy Soc A135:348–375
[26] Kaptay G (2015) The partial surface tension of components of a solution. Langmuir 31:5796–5804
[27] Kaptay G (2022) Extension of the Gibbs-Duhem relation to partial molar surface thermodynamic properties of solutions. Langmuir 39(16):4906
[28] Kaptay G (2008) A unified model for the cohesive enthalpy, critical temperature, surface tension and thermal volume thermal expansion coefficient of liquid metals of bcc, fcc, and hcp crystals. Mater Sci Eng A 495:19–26
[29] J Brillo (2016) Thermophysical properties of multicomponent liquid alloys. walter de Gruyter GmbH, Berlin.
[30] Ansara I, Dinsdale AT, M. H. (1998) Rand, COST 507: thermochemical database for light metal alloys. Off Off Publ Eur Commun 2:297–299
[31] Amore S, Brillo J, Egry I (2011) Experimental measurment of surface tension of of Cu-Ti liquid alloys. High Temp High Press 40:225–235
[32] Brillo J, Kolland G (2016) Surface tension of liquid Al-Au binary alloys. J Mater Sci 51(10):4888. https://doi.org/10.1007/s10853-016-9794-x
[33] Margrave JL, Krishnan S, Hansen GP, Hauge RH (1990) Spectral emissivities and optical properties of electromagnetically levitated liquid metals as functions of temperature and wavelength. High temp sci 29:17–52
[34] Egry I, Diefenbach A, Dreier W, Piller J (2001) Containerless processing in space thermophysical property measurements using electromagnetic levitation. Int J Thermophys 22:569–578
[35] Kobatake H, Brillo J, Schmitz J, Pichon P-Y (2015) Surface tension of binary Al-Si liquid alloys. J Mat Sci 50:3351–3360
[36] Brillo J, Lauletta G, Vaianella L, Arato E, Giuranno D, Novakovic R, Ricci E (2014) Surface tension of liquid Ag-Cu binary alloys. ISIJ Int 54:2115–2119
[37] Soldi L, Quaini A, Gosse S, Brillo J, Roskosz M (2020) Thermodynamic and thermophysical properties of Cu-Si liquid alloys. High Temp High Press 49:155–171
[38] Cummings DL, Blackburn DA (1991) Oscillations of magnetically levitated aspherical droplets. J Fluid Mech 224:395–416
[39] Brillo J, Wessing J, Kobatake H, Fukuyama H (2019) Surface tension of liquid Ti with adsorbed oxygen and its prediction. J Mol Liq 290:1–12

[40] Paradis P-F, Ishikawa T, Lee G-W, Holland-Moritz D, Brillo J, Rhim W-K, Okada JT (2014) Materials properties measurements and particle beam interactions studies using electrostatic levitation. Mater Sci Eng R Rep 76:1–53
[41] Paradis P-F, Rhim W-K (2000) Non-contact measurements of thermophysical properties of titanium at high temperature. J Chem Thermodyn 32:123–133
[42] Okada JT, Ishikawa T, Watanabe Y, Paradis P-F (2010) Surface tension and viscosity of molten vanadium measured with an electrostatic levitation furnace. J Chem Thermodyn 42:856–859
[43] Egry I, Holland-Moritz D, Novakovic R, Ricci E, Wunderlich R, Sobczak N (2010) Thermophysical properties of liquid AlTi-based alloys. Int J Thermophys 31:949–965
[44] D. A. Porter, K. E. Easterling and M. Y. Sherif, (2009) Phase transformations in metals and alloys. T a F Group, Eds Boca Raton: CRC Press
[45] Fedorov P, Volkov S (2016) Chemistry, physics, materials science. Russ J Inorg Chem 61:772–775
[46] Massalski TB (1986) Binary alloy phase diagrams. American Society for Metals
[47] Kostov A, Živković D (2008) Thermodynamic analysis of alloys Ti–Al, Ti–V, Al–V and Ti–Al–V. J Alloy Compd 160:164–171
[48] Allen BC (1963) The surface tension of liquid transition metals at their melting points. Trans AIME 227:1175
[49] Amore S, Delsante S, Kobatake H, Brillo J (2013) Excess volume and heat of mixing in Cu-Ti liquid mixture. J Chem Phys 139:1–6